small
NANO MICRO

Mechanical Frequency and Amplitude Modulation of a Quantum Cascade Laser Integrated with a Plasmonic Nanoantenna

*John Kohoutek, Dibyendu Dey, Alireza Bonakdar, Ryan Gelfand, Vala Fathipour, Omer Gokalp Memis, and Hooman Mohseni**

Surface plasmons (SPs) can be generated at the interface between two materials having opposite signs of dielectric susceptibility.[1] This principle has recently been exploited in many applications, ranging from enhanced optical transmission (EOT),[2] which can be used for enhanced photodetection,[3] biosensing,[4] optical trapping of small particles[5] and bacteria,[6] and even detection of the optical gradient force.[7] Lately, there has been an increased interest in using SP devices for optical modulation,[8] including all-optical modulation.[9,10] SP based devices can also be integrated with other semiconductor technologies, one example being the quantum cascade laser (QCL).[11–13] When the QCL, a semiconductor laser that works based on the principle of intersubband transitions,[14] was invented, it gave the community a compact laser source that worked in the mid to far infrared. The mode of this laser source is very sensitive to the reflectivity of the facets,[10,15] which means that changing the reflectivity of one of these facets gives a viable way to externally modulate the output of the laser source. There has also been a keen interest in using plasmonic integrated QCLs,[11–13] and because many molecules have vibrational resonance in the mid to far infrared,[16] some of these devices may be used for biosensing.[12,13] Recently, an efficient method of chip-scale mechanical tuning of QCL has been demonstrated.[17] Here we experimentally demonstrate an alternative approach, where a small change in the position of an atomic force microscope (AFM) tip with respect to an optical antenna hotspot tunes the laser operating frequency as well as its output power. Because we are using the near field interaction between the apex of the AFM tip with the antenna hot spot to modulate the entire laser, our approach uses a volumetric change that is many orders of magnitude less than previous approaches to modulate the laser output.[17] We have measured the output spectrum and amplitude of the device as a function of AFM tip position over the hotspot, as well as measured the near-field image using a modified apertureless near-field scanning optical microscope.[12,13] Our measurement quantifies the sensitivity of such an antenna integrated device which can potentially be used for molecular sensing.

Our device has been fabricated by defining a metal-dielectric-metal (MDM) based bow-tie antenna structure on the facet of the quantum cascade laser. We have previously optimized the process such that the fabrication reduces the threshold current density by 25% without changing the other laser parameters significantly.[10,12,13] This reduction is mainly due to the increased reflectivity of the gold coated facet.[13] These composite material based nano-antennas have showed an improved performance in terms of near field intensity enhancement over single metal designs.[12,13] First the antenna is designed to strongly couple to the laser modes using full 3D finite-difference-time-domain (FDTD) simulations. The antenna consists of two triangle structures separated by a gap of 100 nm. The fabrication details are discussed in the experimental section.

The AFM tip is placed over the hot-spot of the bow-tie nanoantenna. The measured near-field is shown in **Figure 1**b. The experimental set-up is shown in **Figure 2**. A lock-in amplifier allows us to synchronize two frequencies: the driving frequency of the laser and the frequency of the AFM tip. This allows us to vary the delay of the trigger signal of the QCL driving pulse to measure the spectrum at each vertical position of the AFM tip over the hot spot. A more detailed explanation of the setup can be found in the methods section. The QCL is operated just above the threshold current. The spectrum was recorded at 6 equidistant delay points between 0 and 2π with respect to the AFM tip cycle. The time resolved step-scan for all measurements is shown in **Figure 3**. As the delay was varied, the central frequency of operation of the laser shifted. In effect, this has created mechanical frequency modulation in the laser device.

The time resolved step-scan showing 50 ns of laser operation is shown in Figure 3. The figure also shows normalized amplitude of the step scan measurement so that one can see the shift of lasing frequency with varying delay which corresponds to the varying position of the AFM tip. In this mode of operation we have recorded the frequency shift when

Dr. J. Kohoutek, Dr. D. Dey, A. Bonakdar, R. Gelfand, V. Fathipour, Dr. O. G. Memis, Prof. H. Mohseni
Bio-Inspired Sensors and Optoelectronics Laboratory (BISOL), EECS
Northwestern University
2145 Sheridan Rd., Evanston, IL 60208 USA
E-mail: hmohseni@ece.northwestern.edu

DOI: 10.1002/smll.201200800

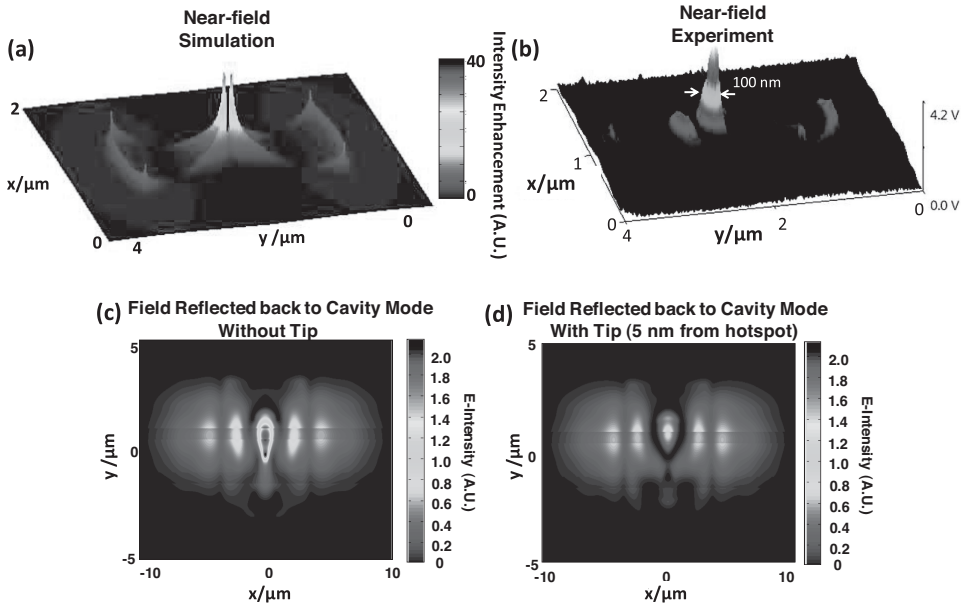

Figure 1. a) 3D simulation showing the intensity enhancement above the antenna at resonance condition. b) 3D NSOM image showing the squeezing optical mode of the device. Full-width at half-maximum (FWHM) was found to be ≈100 nm. c) Reflected field intensity inside core of QCL without AFM tip near hot spot. d) Reflected field intensity with tip near hot spot.

the AFM tip moves with an amplitude of ≈50 nm toward and away from the hotspot and recorded a signal amplitude modulation of 33.3%. We also experimentally observed more than 74% laser power variation when an AFM tip is moved near and away from the hotspot laterally (distance of micrometers) as shown in **Figure 4**. Thus, a small variation of the AFM tip position can change the output of the laser significantly due to the strong influence of the plasmonic modes on the laser cavity modes. This behavior is very interesting, because without the strong influence of the nanoantenna, the emitted light at $\lambda = 6.1$ μm would not be significantly scattered by an object that is ≈60 times smaller than its wavelength. Also, the motion of such a small scattering point by a small amount (≈λ/120) would only lead to an extremely small change of laser output. Without the antenna this interaction would have produced a nearly four orders of magnitude less amplitude change according to our simulations, a change of only 0.007%.

In order to explain the experimental observation, we have solved the rate equations[15] that govern the density of carriers in the upper and lower states of the QCL and photon density, since these are rapidly changing near our operating point which is right above the threshold current. The rate equations are given below:

$$\frac{J}{q} - \frac{n_3}{\tau_3} - s g_c (n_3 - n_2) = 0 \quad (1)$$

$$\frac{n_3}{\tau_{32}} + s g_c (n_3 - n_2) - \frac{n_2}{\tau_2} = 0 \quad (2)$$

$$\frac{c}{n_{\text{eff}}} \left(s (g_c (n_3 - n_2) - \alpha) + \beta \frac{n_3}{\tau_{\text{sp}}} \right) = 0 \quad (3)$$

where J is injected current density, q is electron charge, n_3 and n_2 are populations of states 3 and 2, s is photon density, τ is the lifetime for the states and transitions, g_c is the gain cross section, n_{eff} is the effective refractive index, c is the speed of light, α is the loss (addition of mirror and waveguide loss), and β is spontaneous emission factor. The QCL laser parameters we have used to model our QCL are: $n_{\text{eff}} = 3.2$, $\Gamma = 0.5$, $z_{32} = 1.6$ nm, $\gamma_{32} = 25$ meV, $\tau_{32} = 1.4$ ps, $\tau_2 = 0.2$ ps, $\tau_3 = 0.8$ ps, $\alpha_w = 20$ cm^{-1}, where n_{eff}

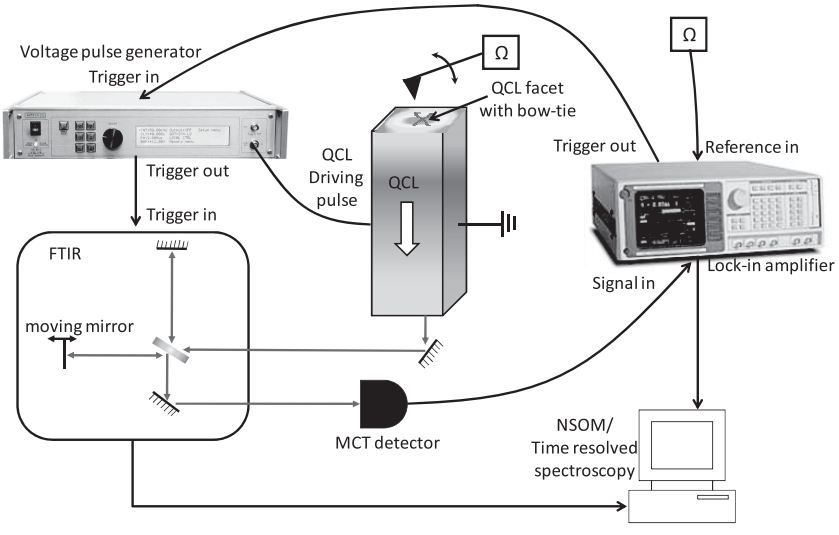

Figure 2. Set-up used to simultaneously measure near-field scanning optical microscopy (NSOM), topography, and time-resolved spectrum of the device.

small 2012,
DOI: 10.1002/smll.201200800

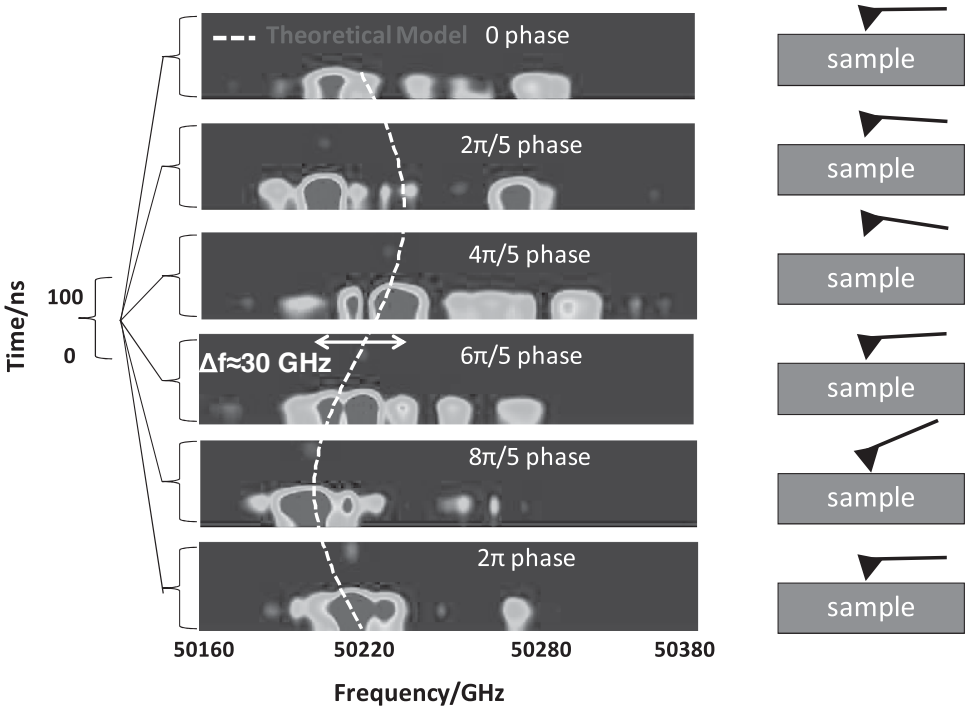

Figure 3. Right: Schematic diagram of the set-up used to measure the spectrum of the laser at different positions of the AFM tip. Left: A shift in laser frequency and amplitude was observed due to feedback from the apex of the vibrating AFM tip. At $2\pi/5$ phase, mode hopping causes the fit line to split the two modes in the figure. The white dotted line shows the calculated theoretical model for the shift in frequency.

is the effective index, z_{32} is the dipole matrix element of the optical transition, γ_{32} is the luminescence linewidth, τ_{32} is the LO-phonon scattering time, τ_3 and τ_2 are the upper and lower state lifetimes, respectively, and α_w is the waveguide loss. The QCL parameters are based on published data[14,18] with a similar active region design to ours and show a good agreement with our experimental threshold current density. The rate equations contain a mirror loss term which contains the reflectivity of each of the facets, one of which was found to be changing through FDTD simulations because of the motion of the AFM tip with respect to the bow-tie antenna. To model our system which is being modified by the moving AFM tip, we have performed FDTD simulations that show a dramatic change in the electric field intensity when we record the field within the QCL waveguide structure (see Figure 1c,d). To calculate the change in reflectivity of the bow-tie antenna, we record the electric and magnetic fields near the back of the device and calculate the reflected power with and without the AFM tip over the hot spot to be 12%. We solved the rate equations self consistently for the photon density *s,* and the state densities n_3 and n_2 as a function of time for a moving tip. The laser output power can change by a maximum of 93%, while we have observed a change of 74%. The difference between these two figures is likely due to imperfections and non-optimal

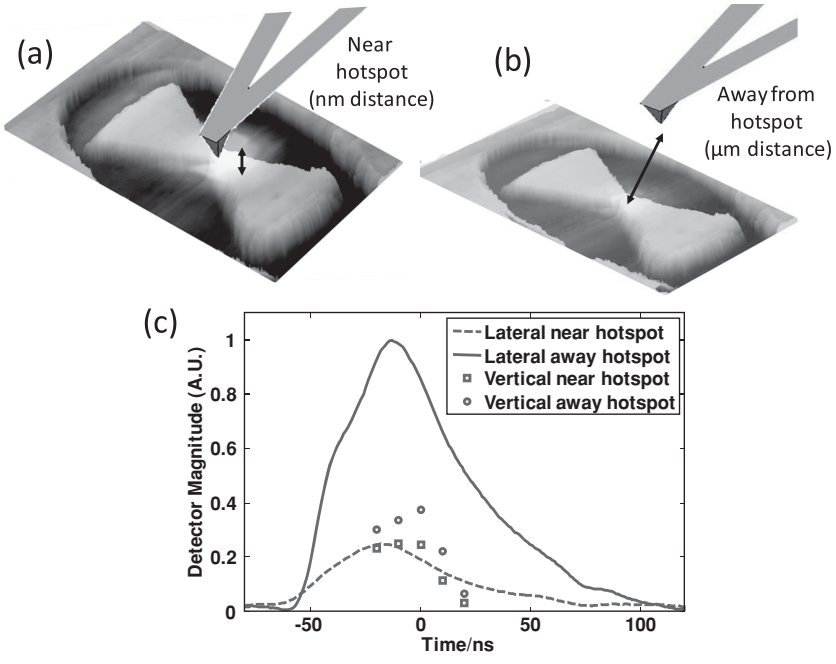

Figure 4. a,b) Composite image of the antenna topography and the schematic of the AFM tip when the AFM tip is near and away from the hot-spot laterally. c) Experimental observation of modulation in near-field intensity signal with varying AFM tip position. When moved vertically (amplitude ≈ 50 nm), the amplitude modulation is ≈33%. When moved laterally (distance of micrometers) the amplitude modulation is nearly 74%.

DOI: 10.1002/smll.201200800

conditions between experimental setup and measurement technique. Thus, the amplitude of the laser is also modulated mechanically. To calculate the change in frequency as a function of time we have taken the rate carriers that produce heat through different non-radiative mechanisms from the rate equations, n_3/τ_3 and n_2/τ_2 and multiplied them by the respective energy of those transitions as well as the heat losses due to photon absorption in the waveguide. We also included the variation of the Joule heat in the laser due to rapid change of laser current density near threshold at a constant bias[19] which gives a term that is the change of current density near threshold times the voltage at our bias point of the QCL (1 percent above threshold) to get the power density lost due to heat in the QCL:

$$P_{\text{heat}} = L \times w \times d \left(\frac{n_3}{\tau_3} \frac{hc}{\lambda_0} + \frac{n_2}{\tau_2} 2\hbar\omega_{\text{LO}} + s\alpha_{\text{W}} \frac{c}{n_{\text{eff}}} \frac{hc}{\lambda_0} + \frac{\Delta J\, V_{\text{app}}}{d} \right) \quad (4)$$

where L is the length of the cavity, w and d are the width and height of the active region, h is Planck's constant $\hbar\omega_{\text{LO}}$ is the LO phonon resonance energy (30 meV), multiplied by two because the active region of our design generates two phonons per transition, λ_0 is the operating wavelength (6.1 μm), ΔJ is the change in current density near threshold (defined as point of maximum positive second derivative in current-power plot), and V_{app} is the applied voltage. Then, we have calculated the change in core temperature when considering this power term and the thermal resistance of the laser.[20] The core temperature is found to be varying as a function of time, due to the time varying terms in the P_{heat} equation, originally coming from the laser facet change in reflectivity. Finally we have used the relation $\Delta k = \Delta T k (b + a n_{\text{eff}})/n_{\text{eff}}$ to find the change in wavenumber as a function of time, and converted to frequency.[21] Here, k is wavenumber in cm^{-1} converted to Δf–frequency in GHz, b is temperature coefficient of change in refractive index (5.9×10^{-4}), and a is linear thermal expansion coefficient ($5.54 \times 10^{-6}\ \text{K}^{-1}$).[21] The results of this calculation show a final Δf of 31.8 GHz, in good agreement with our experimental data.

In non-contact mode operation, the AFM tip has an oscillation amplitude of ≈50 nm toward and away from the hotspot, and there is never a point of contact with the surface. The calculated figure of merit of the system is $g = \Delta f/\Delta d \approx 6.4 \times 10^8\ \text{Hz nm}^{-1}$. Although the previous external mechanical frequency tuned QCL show a larger relative tuning range, the g value of the device was on the order of $\approx 2.7 \times 10^7\ \text{Hz nm}^{-1}$ which is an order of magnitude less than what we report here. In parallel, our device requires approximately five orders of magnitude less volumetric change per λ^3. We believe that the reason for the higher g in our device versus the previous design is the high mode confinement via the plasmonic nanoantenna and the strong coupling of that mode to the cavity mode of the QCL. When the plasmonic mode is modified by the AFM tip, it strongly changes the cavity mode of the laser through this strong coupling. Both devices differ from previous designs that use the optical gradient force to modulate the frequency.[22] In those cases, the devices can actually be mechanically self-actuated by the optical gradient force, while the devices discussed here are externally actuated.

In conclusion, the laser cavity mode has shown an extremely high sensitivity with respect to the position of the probing AFM tip over the optical antenna hotspot. The laser power is reduced by ≈74% and shifts by nearly 30 GHz with a change in the AFM tip position near the hot-spot, creating mechanical frequency and amplitude modulation. We have developed a theoretical model based on the rate equations for a QCL and dynamic mirror reflectivity that confirm our experiments. This strong influence relies on a metal-dielectric-metal plasmonic bow-tie antenna integrated onto the facet of a QCL which can squeeze the optical mode to within a spot size of ≈100 nm; this is 60 times smaller than the operating wavelength. We used finite-difference-time-domain (FDTD) software to optimize the design of such a device and measured it using a modified apertureless near-field scanning optical microscope (a-NSOM), which can also measure the amplitude and spectrum of the device as a function of time and AFM tip position. We have compared our device to a previous frequency modulated QCL[17] and calculated a figure of merit which is an order of magnitude higher while our design uses a volumetric change per λ^3 that is five orders of magnitude smaller. Our device differs from optical gradient force actuated devices in that our devices is externally mechanically actuated while those devices are self actuated through the optical force.[22] This sensitivity of the laser cavity mode to the fine position of a nanometer-scale metallic absorber opens up the opportunity for modulating large amount of optical power by changing the optical properties of a miniscule volume in an integrated, chip-scale device.

Experimental Section

For the simulation, a plane wave with wavelength 6.1 μm (operating wavelength of the device) was launched from the inside of the laser core material at normal incidence to the surface. All material data used in the simulation were from ref.[23] For the laser core, a weighted average (3.2) of the refractive index of InGaAs/InAlAs was used, which constituted the active layers of the QCL. To find the resonant length of each arm of the bow-tie, the peak intensity enhancement was simulated at the antenna gap on the same level as the top surface as a function of the length of each arm of the bow-tie. To achieve better accuracy, a very fine mesh size near the antenna region was used. Perfectly matched layer (PML) boundary conditions were employed across the simulation boundary. The simulated field intensity was an integrated average over the volume (100 nm^3) near the antenna gap. The antenna was resonant at a length of the arm of ≈1.75 μm. The gap between two bow-tie arms was kept to be 100 nm for all simulations.

After optimizing the design, the MDM bow-tie structure was fabricated on the coated facet of the QCL using a focused ion beam (Hellios FEI). The fabrication details for this device have been described previously.[12,24] The plasmonic mode that resonates with the optical antenna exists only in the near field and thus cannot be studied with an ordinary microscope. Previously, a backscattered apertureless near-field scanning optical microscope was used to study the near field of the device (a-NSOM).[25]

DOI: 10.1002/smll.201200800

However, for this work, a modified a-NSOM, which could also simultaneously measure the spectrum of the device with respect to time and AFM tip position, was used. During the measurement, the laser was operated in pulsed mode and biased using a voltage pulse generator and enclosed in a temperature and airflow stabilized environment. To observe the lasing spectrum at a specific position of the AFM tip, both the voltage pulse generator and the FTIR were synchronized with the AFM tip's vibration frequency. A lock-in amplifier allows synchronization of these two frequencies in the following way. First, the amplitude signal from the AFM was fed into the reference input of the lock-in. Next, the trigger-out of the lock-in was fed into the trigger-in of the voltage pulse generator. Finally, the high voltage pulse from the voltage pulse generator was used to pulse the QCL device, while the trigger-out signal from the pulse generator is simultaneously used to trigger the FTIR. The voltage pulse generator allows the delay of the pulse sent to the laser to be varied with respect to the AFM trigger signal. This allows measurement of the spectrum at different vertical positions of the AFM tip over the hot spot. The spectrum was recorded at 6 equidistant delay points between 0 and 2π with respect to the AFM tip cycle. The time-resolved step-scan for all measurements is shown in Figure 3. As the delay was varied, the central frequency of operation of the laser shifted. In effect, this created mechanical frequency modulation in the laser device. The set-up has been elaborated in Figure 2, where the apex of the vibrating AFM tip scatters back the near-field light intensity through the laser and is collected using a liquid-nitrogen cooled mercury-cadmium-telluride (MCT) detector. The background noise removal and near-field imaging details can be found in previous publications.[12,24] A research-grade Fourier transform infrared spectrometer (FTIR) was included in the set-up to simultaneously measure the spectrum of the device. As the natural vibration frequency of the AFM tip was measured to be ≈90 kHz (Ω), each tip position repeated itself at an interval of ≈11.1 μs (Ω^{-1}). The resolution of the time-resolved measurement was kept at 10 ns, thereby recording 5 sets of spectral data for an operating pulse width of 50 ns.

Acknowledgements

J.K. and D.D. contributed equally to this work. This work was partly supported by projects CBET-0932611 and EECS-0621887 under the National Science Foundation (NSF) and project W911NF-11-1-0390 under the Army Research Office (ARO). The authors are also grateful to the Materials Processing and Crystal Growth Facility and NUANCE facility at Northwestern University for fabrication and SEM characterizations.

[1] H. Raether, *Surface plasmons on smooth and rough surfaces and on gratings*, Springer, New York **1988**.
[2] T. W. Ebbesen, H. J. Lezec, H. F. Ghaemi, T. Thio, P. A. Wolff, *Nature* **1998**, *391*, 667.
[3] W. Wu, A. Bonakdar, H. Mohseni, *Appl. Phys. Lett.* **2010**, *96*.
[4] R. M. Gelfand, L. Bruderer, H. Mohseni, *Opt. Lett.* **2009**, *34*, 1087.
[5] M. Righini, A. S. Zelenina, C. Girard, R. Quidant, *Nat. Phys.* **2007**, *3*, 477.
[6] M. Righini, P. Ghenuche, S. Cherukulappurath, V. Myroshnychenko, F. J. G. de Abajo, R. Quidant, *Nano Lett.* **2009**, *9*, 3387.
[7] a) J. Kohoutek, D. Dey, A. Bonakdar, R. Gelfand, A. Sklar, O. G. Memis, H. Mohseni, *Nano Lett.* **2011**, *11*, 3378; b) G. Volpe, R. Quidant, G. Badenes, D. Petrov, *Phys. Rev. Lett.* **2006**, *96*.
[8] M. J. Dicken, L. A. Sweatlock, D. Pacifici, H. J. Lezec, K. Bhattacharya, H. A. Atwater, *Nano Lett.* **2008**, *8*, 4048.
[9] a) R. A. Pala, K. T. Shimizu, N. A. Melosh, M. L. Brongersma, *Nano Lett.* **2008**, *8*, 1506; b) N. Large, M. Abb, J. Aizpurua, O. L. Muskens, *Nano Lett.* **2010**, *10*, 1741; c) J. A. Dionne, K. Diest, L. A. Sweatlock, H. A. Atwater, *Nano Lett.* **2009**, *9*, 897.
[10] J. Kohoutek, A. Bonakdar, R. Gelfand, D. Dey, I. H. Nia, V. Fathipour, O. G. Memis, H. Mohseni, *Nano Lett.* **2012**, *12*, 2537.
[11] a) N. Yu, E. Cubukcu, L. Diehl, M. A. Belkin, K. B. Crozier, F. Capasso, D. Bour, S. Corzine, G. Hofler, *Appl. Phys. Lett.* **2007**, *91*, 173113; b) N. Yu, E. Cubukcu, L. Diehl, D. Bour, S. Corzine, J. Zhu, G. Hoefler, K. B. Crozier, F. Capasso, *Opt. Express* **2007**, *15*, 13272.
[12] D. Dey, J. Kohoutek, R. M. Gelfand, A. Bonakdar, H. Mohseni, *IEEE Photonics Technol. Lett.* **2010**, *22*, 1580.
[13] D. Dey, J. Kohoutek, R. M. Gelfand, A. Bonakdar, H. Mohseni, *Opt. Lett.* **2010**, *35*, 2783.
[14] J. Faist, F. Capasso, D. L. Sivco, C. Sirtori, A. L. Hutchinson, A. Y. Cho, *Science* **1994**, *264*, 553.
[15] H. C. Liu, F. Capasso, *Intersubband Transitions in Quantum Wells: Physics and Device Applications II*, Academic Press, San Diego **2000**.
[16] M. Tonouchi, *Nat. Photonics* **2007**, *1*, 97.
[17] Q. Qin, B. S. Williams, S. Kumar, J. L. Reno, Q. Hu, *Nat. Photonics* **2009**, *3*, 732.
[18] a) J. Faist, F. Capasso, C. Sirtori, D. L. Sivco, J. N. Baillargeon, A. L. Hutchinson, S. N. G. Chu, A. Y. Cho, *Appl. Phys. Lett.* **1996**, *68*, 3680; b) C. Gmachl, F. Capasso, D. L. Sivco, A. Y. Cho, *Rep. Prog. Phys.* **2001**, *64*, 1533; c) C. Sirtori, J. Faist, F. Capasso, D. L. Sivco, A. L. Hutchinson, S. N. G. Chu, A. Y. Cho, *Appl. Phys. Lett.* **1996**, *68*, 1745.
[19] a) C. Sirtori, F. Capasso, J. Faist, A. L. Hutchinson, D. L. Sivco, A. Y. Cho, *IEEE J. Quantum Electron.* **1998**, *34*, 1722; b) D. K. Guo, L. E. Cheng, X. Chen, F. S. Choa, J. Y. Fan, T. Worchesky, *J. Appl. Phys.* **2011**, 109.
[20] a) L. A. Coldren, S. W. Corzine, *Diode Lasers and Photonic Integrated Circuits*, John Wiley and Sons, Inc., New York **1995**; b) C. Gmachl, A. M. Sergent, A. Tredicucci, F. Capasso, A. L. Hutchinson, D. L. Sivco, J. N. Baillargeon, S. N. G. Chu, A. Y. Cho, *IEEE Photonics Technol. Lett.* **1999**, *11*, 1369; c) Y. M. Kim, M. J. W. Rodwell, A. C. Gossard, *J. Electron. Mater.* **2002**, *31*, 196.
[21] D. Dey, W. Wu, O. G. Memis, H. Mohseni, *Appl. Phys. Lett.* **2009**, *94*.
[22] D. Van Thourhout, J. Roels, *Nat. Photonics* **2010**, *4*, 211.
[23] E. D. Palik, *Handbook of Optical constants of solids*, Academic Press, New York **1985**.
[24] D. Dey, J. Kohoutek, R. M. Gelfand, A. Bonakdar, H. Mohseni, *Opt. Lett.* **2010**, *35*, 2783.
[25] a) R. Hillenbrand, B. Knoll, F. Keilmann, *J. Microsc. (Oxford, UK)* **2001**, *202*, 77; b) E. Cubukcu, N. F. Yu, E. J. Smythe, L. Diehl, K. B. Crozier, F. Capasso, *IEEE J. Sel. Top. Quantum Electron.* **2008**, *14*, 1448.

Received: April 13, 2012
Revised: June 19, 2012
Published onine: